

RESEARCH ARTICLE

Influence of rotation on peristaltic flow for pseudoplastic fluid: a wavy channel

Hayat Adel Ali ^{a*}, Mohammed R. Salman ^b

^aDepartment of Applied Science, University of Technology-Iraq, Baghdad, Iraq

^bDepartment of Mathematics, University of Kerbala, Kerbala, Iraq

hayat.A.Ali@uotechnology.edu.iq, mohammed.razaq@uokerbala.edu.iq

ARTICLE INFO

Article History:

Received 4 January 2024

Accepted 9 June 2024

Available Online 10 October 2024

Keywords:

Peristaltic transport

Pseudoplastic fluid

Rotation force

Wavy channel

AMS Classification 2010:

76D05; 76D07; 76N10

ABSTRACT

The phenomenon of rotation serves multiple purposes in cosmic and geophysical phenomena. It offers insights into the formation of galaxies and the circulation patterns of oceans. Moreover, rotational diffusion elucidates the orientation of nanoparticles within fluid mediums. Investigating the dynamics of fluid peristalsis under the influence of rotational forces holds significant relevance in addressing challenges associated with the transportation of conductive physiological fluids such as blood, polymeric materials, and saline water. This study focused on studying the impact of rotation on the peristaltic transport of non-Newtonian pseudoplastic fluids through a wavy channel. The complexity of flow equations, including the continuity and motion equations, is mathematically formulated and transformed into dimensionless nonlinear ordinary differential equations depending on the assumption of low Reynolds number and long wavelength approximation. Perturbation technique is employed to solve the problem for the stream function and the resulted system is implemented and plotted using MATHEMATICA software along with the boundary conditions. Graphical discussion is involved to utilize the impact of the emerging parameters in the flow characteristic, encompassing the velocity profile, pressure gradient, pressure rise, and trapping phenomenon. The research revealed that rotation significantly influences the fluid flow within the channel, diminishing the regressive and inhibitory impact of the fluid parameter, consequently enhancing the fluid flow within the channel.



1. Introduction

Extensive research has been conducted on peristaltic motion in recent years due to the fact that it involves the study of wave-like motion in physiological fluids resulting from interaction with surrounding boundaries. Such phenomena are evident during the process of food ingestion through the esophagus, the propagation of lymphocytes within the lymphatic system, the circulation of blood through vessels, the movement of urine toward the bladder, and numerous other instances that collectively contribute to our understanding of peristalsis. Moreover, peristaltic transport has

wide applications in medical engineering, science, and modern industry, such as aggressive chemicals, high solid slurries, noxious fluids (nuclear industries), heart-lung machines, blood pump machines, and dialysis machines [1–4]. The initial effort to elucidate this phenomenon was attributed to [5]. Subsequent to this progress, numerous studies, delving into the exploration of peristaltic flow of various fluid types under diverse influencing factors, were illustrated by many researchers. [6] discussed the impact of long wavelengths and the low Reynolds number assumption on peristaltic pumping. [7] determined the impact

*Corresponding Author

of the elastic wall of a hollow cylinder's channel of Jeffrey's fluid by peristaltic flow. [8] studied the heat transfer analysis of magnetohydrodynamic (MHD) peristaltic transport of Jeffrey fluid in an inclined tapered asymmetric channel. For more information, see [9–13].

Non-Newtonian fluids, including molten plastics, artificial fibers, polymeric materials, food-stuffs, blood, slurries, and synovial liquids, exhibit shear-stress-strain relationships that diverge significantly from the traditional viscous model, finding numerous applications in manufacturing and commerce [14–17]. Significant literature exists on the study of peristaltic motion in the presence of non-Newtonian fluids. Many of these types of fluids exhibit characteristics of shear-thinning yield stress materials [18], such as pseudoplastic fluid which is found in blood plasma, latex paint, polymer solutions, and similar solutions of high molecular weight substances. At low shear rates, these fluids experience the formation of shear stress that results in the reordering of the molecules to reduce the overall stress. [9] analyzed the impact of Soret and Dufour on the peristaltic flow of magnetohydrodynamic (MHD) pseudoplastic nanofluid in a tapered asymmetric channel. The impact of pseudoplasticity and dilatancy of fluid on the peristaltic flow of non-Newtonian fluid in a non-uniform asymmetric channel was investigated [19]. In 2014, [20] studied the impact of wall properties and slip conditions on the peristaltic flow of pseudoplastic fluid in a curved channel. An effect of magnetohydrodynamic (MHD) and thermal radiation on the peristaltic flow of a pseudoplastic nanofluid through a porous medium asymmetric canal with convection boundary conditions was depicted by [21].

A rotational phenomenon plays a pivotal role in various cosmic and geophysical phenomena. It aids in comprehending the emergence of galaxies and the circulation of oceans. Nanoparticles' orientation in fluids is attributed to rotational diffusion. Moreover, rotation is noteworthy in specific flow scenarios within physiological fluids like saline water and blood. This synergy of rotation facilitates the movement of biological fluids within the intestines, ureters, and arterioles. Several studies focused on the rotational system's impact on the peristaltic flow of various fluids. [22] analyzed the flow of non-Newtonian fluid with a porous medium under the effect of rotation and magnetic force. [23] was concerned with the peristaltic flow of a Jeffrey fluid in an asymmetric rotating channel. [24] illustrated the

influence of magnetic force, rotation, and nonlinear heat radiation on the peristaltic transport of hybrid bio-nanofluids through a symmetric channel. [25] investigated the peristaltic flow of Bingham plastic fluid under the effect of rotation and induced magnetic field. For more information, see Refs. [26–30].

Lately, there has been a lack of attention given to studying peristaltic flows under conditions where both the fluid and the channel experience solid body rotation, i.e., the entire system, comprising both the fluid and the channel, is situated within a rotating frame characterized by a consistent angular velocity. The aforementioned studies have primarily focused on peristaltic flows involving different non-Newtonian fluids, addressing rotational effects. Nevertheless, there remains a gap in the previous literature concerning the impact of the rotation frame on the peristaltic transport of pseudoplastic fluids. In this study, We extended the inquiry delineated in [19] by elucidating the physical alterations observed in our fluid during the flow, which experiences a reduction in viscosity as the shear rate increases during rotation. As a consequence, its velocity increases, which finds application in various contexts such as in blood apheresis machine and water treatment. In this article, physical modeling governing the equation of peristaltic flow of pseudoplastic under the effect of rotation is described and reduced to the differential equation by using long wavelength and low Reynolds number assumptions. The closed-form analytic solution for the stream function and fluid velocity is provided. Subsequently, a graphical analysis is conducted using codes from the Mathematica package to illustrate the impact of key parameters on flow characteristics.

2. Mathematical model of the problem

Assuming the incompressible peristaltic motion of a non-Newtonian, electrically conducting, pseudoplastic fluid through a two-dimensional asymmetric a wavy channel of width $2d$ in which the channel rotates about the horizontal with uniform angular velocity Ω see Fig. 1. The induced sinusoidal propagation waves of wavelength λ are advancing with a constant speed c in the \bar{X} - axis, and the \bar{Y} -axis is normal to it.

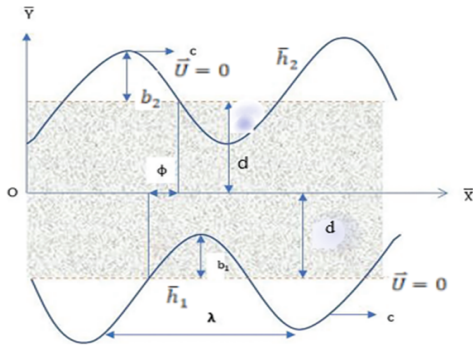


Figure 1. Geometry of problem

The mathematical equations for the channel walls are provided as follows [25]:

$$\bar{Y} = \bar{h}_1(\bar{X}, \bar{t}) = d + b_1 \sin\left(\frac{2\pi}{\lambda}(\bar{X} - c\bar{t})\right), \quad (1)$$

$$\bar{Y} = \bar{h}_2(\bar{X}, \bar{t}) = -d - b_2 \sin\left(\frac{2\pi}{\lambda}(\bar{X} - c\bar{t}) + \phi\right). \quad (2)$$

where \bar{h}_1 and \bar{h}_2 are the lower and upper walls respectively, b_1 and b_2 denote the waves' amplitudes, \bar{t} stands for time, $\phi \in [0, \pi]$ and represents the phase difference. When $\phi = 0$, it indicates waves out of phase for a symmetric channel, and when $\phi = \pi$ the waves are in phase. Additionally, the values of d, b_1, b_2 and ϕ satisfy the inequality.

$$b_1^2 + b_2^2 + b_1 b_2 \cos \phi \leq (d)^2, \quad (3)$$

The governing equations for an incompressible fluid in the fixed frame are formulated as follows: The continuity equation is:

$$\nabla \cdot \vec{V} = 0, \quad (4)$$

The motion equation is:

$$\rho \left(\frac{\partial \vec{V}}{\partial t} + (\vec{V} \cdot \nabla) \vec{V} \right) + \rho [\Omega \times (\Omega \times \vec{V}) + 2\Omega \times \vec{V}] = -\nabla \bar{P} + \nabla \cdot \bar{S}, \quad (5)$$

Associated with the no-slip boundary condition bellows:

$$\vec{U} = 0 \text{ at } \bar{h}_1 \text{ and } \bar{h}_2. \quad (6)$$

In which $\vec{V} = (\bar{U}, \bar{V})$ is the fluid velocity vector in \bar{X} and \bar{Y} coordinates respectively, ρ, \bar{P} are the fluid density and the pressure, $\vec{\nabla} = \left(\frac{\partial}{\partial \bar{X}}, \frac{\partial}{\partial \bar{Y}} \right)$ is the gradient vector, $\rho(\Omega \times (\Omega \times \vec{V}))$ denotes the centrifugal force while the term $\rho(2\Omega \times \vec{V})$ refers to the Coriolis force, \bar{S} is the Cauchy stress tensor

for pseudoplastic fluid which defined as [9,19]:

$$\bar{S} + \lambda^*_{1} \left(\frac{\partial \bar{S}}{\partial t} - \nabla \vec{V} \cdot \bar{S} - \bar{S} \cdot (\nabla \vec{V})^T \right) + \frac{1}{2} (\lambda^*_{1} - \mu^*_{1}) (\check{A}_1 \bar{S} + \bar{S} \check{A}_1) = \mu \check{A}_1, \quad (7)$$

$$\check{A}_1 = \nabla \vec{V} + (\nabla \vec{V})^T. \quad (8)$$

where μ is the fluid viscosity, λ^*_{1}, μ^*_{1} are the relaxation times, \check{A}_1 is the first Rivlin- Ericksen tensor. Consider the wave frame (\bar{x}, \bar{y}) traveling with speed c away from the laboratory frame. The transformation of coordinates and flow properties between fixed and wave frame is given by:

$$\bar{x} = \bar{X} - c\bar{t}, \bar{y} = \bar{Y}, \bar{u} = \bar{U} - c, \bar{v} = \bar{V}, \bar{p}(\bar{x}) = \bar{p}(\bar{X}, \bar{t}). \quad (9)$$

Now, defining the dimensionless parameters and variables in the following manner.

$$\begin{aligned} x &= \frac{\bar{x}}{\lambda}, y = \frac{\bar{y}}{d}, u = \frac{\bar{u}}{c}, v = \frac{\bar{v}}{c}, h_1 = \frac{\bar{H}_1(X)}{d}, \\ h_2 &= \frac{\bar{H}_2(X)}{d}, d = \frac{d_2}{d_1}, \delta = \frac{d}{\lambda}, a = \frac{b_1}{d}, b = \frac{b_2}{d}, \\ \lambda_1 &= \frac{c\lambda^*_1}{d}, p = \frac{d^2 \bar{p}}{\lambda \mu c}, Re = \frac{\rho c d}{\mu}, s_{ij} = \frac{d}{\mu c} \bar{S}_{ij}, \\ \mu_1 &= \frac{c\mu^*_1}{d}, \Omega = \frac{b_1^2 \bar{\Omega}}{\mu}, Ta = \frac{\Omega d Re}{c}. \end{aligned} \quad (10)$$

where Re and δ are the Reynolds number and the dimensionless number of waves respectively. Introducing the dimensionless stream function $\psi(x, y)$, in which,

$$u = \frac{\partial \psi}{\partial y}, v = -\delta \frac{\partial \psi}{\partial x}. \quad (11)$$

The continuity equation is identically achieved. By substituting Eq. (9) and Eq. (10) into Eqs. (2 - 7), we get:

$$\begin{aligned} Re \delta \left((u + 1) \frac{\partial u}{\partial x} + v \frac{\partial u}{\partial y} \right) - 2 Ta (u + 1) = \\ - \frac{\partial p}{\partial x} + \delta \frac{\partial s_{xx}}{\partial x} + \frac{\partial s_{xy}}{\partial y}, \end{aligned} \quad (12)$$

$$\begin{aligned} Re \delta^2 \left((u + 1) \frac{\partial v}{\partial x} + v \frac{\partial v}{\partial y} \right) - 2 Ta \delta v = - \frac{\partial p}{\partial y} + \\ \delta \frac{\partial s_{yy}}{\partial y} + \delta^2 \frac{\partial s_{yx}}{\partial x} - \frac{1}{\kappa} \delta^2 v, \end{aligned} \quad (13)$$

$$s_{xx} + \lambda_1 \left(\delta \left(u \frac{\partial s_{xx}}{\partial x} + v \frac{\partial s_{xx}}{\partial y} \right) - 2\delta s_{xx} \frac{\partial u}{\partial x} - 2s_{xy} \frac{\partial u}{\partial y} \right) + \frac{1}{2} (\lambda_1 - \mu_1) \left(2s_{xy} \left(\frac{\partial u}{\partial y} + \delta^2 \frac{\partial v}{\partial x} \right) + 4\delta s_{xx} \frac{\partial u}{\partial x} \right) = 2\delta \frac{\partial u}{\partial y}, \quad (14)$$

$$\psi = -\frac{F}{2}, \psi_y = 0 \text{ at } y = h_1(x), \quad (23)$$

$$\psi = \frac{F}{2}, \psi_y = 0 \text{ at } y = h_2(x). \quad (24)$$

$$s_{xy} + \lambda_1 \left(\delta \left(u \frac{\partial s_{xy}}{\partial x} + v \frac{\partial s_{xy}}{\partial y} \right) - \delta^2 s_{xx} \frac{\partial v}{\partial x} - s_{yy} \frac{\partial u}{\partial y} \right) + \frac{1}{2} (\lambda_1 - \mu_1) (s_{xx} + s_{yy}) \left(\frac{\partial u}{\partial y} + \delta^2 \frac{\partial v}{\partial x} \right) = \frac{\partial u}{\partial y} + \delta^2 \frac{\partial v}{\partial x^2}, \quad (15)$$

where $h_1(x) = 1 + a \sin(2\pi x)$ and $h_2(x) = 1 + b \sin(2\pi x + \Phi)$.

where $\xi = (\lambda_1^2 - \mu_1^2)$ is the Pseudoplastic fluid parameter.

The parameter F refers to the dimensionless mean flows and it is given by:

$$F = \int_{h_1}^{h_2} u(x, y) dy = \int_{h_1}^{h_2} \frac{\partial \psi}{\partial y} dy = \psi(h_2) - \psi(h_1), \quad (25)$$

$$s_{yy} + \lambda_1 \left(\delta \left(u \frac{\partial s_{yy}}{\partial x} + v \frac{\partial s_{yy}}{\partial y} \right) - 2\delta s_{xx} \frac{\partial v}{\partial y} + 2\delta^2 s_{xy} \frac{\partial v}{\partial x} \right) + \frac{1}{2} (\lambda_1 - \mu_1) \left(2s_{xy} \left(\frac{\partial u}{\partial y} + \delta^2 \frac{\partial v}{\partial x} \right) + 4\delta s_{yy} \frac{\partial v}{\partial y} \right) = 2\delta \frac{\partial v}{\partial y}. \quad (16)$$

Additionally, the connection between F and the nondimensional mean flows in the moving frame, θ , can be derived as:

$$F = \theta + a \sin(2\pi x + \Phi) + b \sin(2\pi x). \quad (26)$$

The pressure rise per unit wavelength is:

$$\Delta p = \int_0^1 \frac{dp}{dx} dx. \quad (27)$$

Employing Eq. (11) and assuming a low Reynolds number and a large wavelength approximation ($\delta \ll 1$), Eqs. (12 - 16) are reduced as follows:

$$\frac{\partial p}{\partial x} = \frac{\psi_{yy}}{(1 + \xi (\psi_{yy})^2)} + 2Ta \left(\frac{\partial \psi}{\partial y} + 1 \right), \quad (17)$$

$$\frac{\partial p}{\partial y} = 0. \quad (18)$$

Through Eq. (18), we conclude that pressure is not a function of y , i.e., $P \neq P(y)$. Neglecting pressure from Eq. (17), we get:

$$\psi_{yyyy} + 3\xi (\psi_{yy})^2 \psi_{yyy} + 6\xi (\psi_{yyy})^2 \psi_{yy} + 2Ta \psi_{yy} = 0, \quad (19)$$

$$s_{xx} = (\lambda_1 + \mu_1) \frac{(\psi_{yy})^2}{(1 + \xi (\psi_{yy})^2)^2}, \quad (20)$$

$$s_{xy} = \frac{\psi_{yy}}{(1 + \xi (\psi_{yy})^2)}, \quad (21)$$

$$s_{yy} = -(\lambda_1 - \mu_1) \frac{(\psi_{yy})^2}{(1 + \xi (\psi_{yy})^2)^2}. \quad (22)$$

Linked to the subsequent dimensionless boundary condition.

3. Solution of the problem

Eq. (19) poses a complex nonlinear differential challenge, rendering an exact solution unattainable. In the field of fluid science, various techniques [31–37] are available to find the desired solution. Therefore, we turn to perturbation technique to calculate series solutions when dealing with a small parameter. Consequently, we applied perturbation to stream function ψ and dimensionless mean flow F , considering them up to the first order with respect to the Pseudoplastic fluid parameter ξ as:

$$\psi = \psi_0 + \xi \psi_1 + O(\xi^2), \quad (28)$$

$$F = F_0 + \xi F_1 + O(\xi^2). \quad (29)$$

3.1. Zeroth order system

$$\psi_{0yyyy} + 2Ta \psi_{0yy} = 0, \quad (30)$$

With the boundary conditions.

$$\psi_0 = -\frac{F_0}{2}, \psi_{0y} = 0, \text{ at } y = h_1(x), \quad (31)$$

$$\psi_0 = \frac{F_0}{2}, \psi_{0y} = 0 \text{ at } y = h_2(x). \quad (32)$$

where

$$F_0 = \theta + a \sin(2\pi x + \Phi) + b \sin(2\pi x). \quad (33)$$

3.2. First order system

$$\begin{aligned} \psi_{1yyyy} + 3(\psi_{0yy})^2 \psi_{0yyyy} + \\ 6(\psi_{0yyy})^2 \psi_{0yy} + 2Ta\psi_{1yy} = 0, \end{aligned} \quad (34)$$

With the following boundary conditions.

$$\psi_1 = -\frac{F_1}{2}, \psi_{1y} = 0, \text{ at } y = h_1(x), \quad (35)$$

$$\psi_1 = \frac{F_1}{2}, \psi_{1y} = 0, \text{ at } y = h_2(x). \quad (36)$$

Solving the two resulting systems by writing suitable codes in Mathematica software, the explicit expression of stream functions ψ_0 and ψ_1 obtained.

$$\psi_0(x, y) = \frac{e^{-\sqrt{A}y} (e^{2\sqrt{A}y}c_1 + c_2)}{A} + c_3 + yc_4, \quad (37)$$

$$\begin{aligned} \psi_1(x, y) = c_7 + yc_8 + \frac{1}{8A}e^{-3\sqrt{A}y} (-c_2^3 + \\ 30c_1c_2^2e^{2\sqrt{A}y} + 30c_1^2c_2e^{4\sqrt{A}y} - c_1^3e^{6\sqrt{A}y} + \\ 8e^{4\sqrt{A}y}c_5 + 8e^{2\sqrt{A}y}c_6 - 6c_1c_2e^{2\sqrt{A}y} (-c_2 + \\ c_1e^{2\sqrt{A}y}) \log(e^{2\sqrt{A}y})). \end{aligned} \quad (38)$$

where $A = -2Ta$, and the coefficients $c_1, c_2, c_3, c_4, c_5, c_6, c_7$ and c_8 consist of complex expressions that will not be detailed here.

4. Results analysis and discussion

In this section, we examine the outcomes of different physical parameters by utilizing the visual representations provided. The analysis includes the variation in the velocity profile, the gradient of pressure, the pressure rise and the trapping phenomenon as a result of the increase in the values of the rotation parameter Ta , the pseudoplastic fluid parameter ξ , the non-dimensional mean flows θ , the phase difference parameter Φ , the lower wall amplitude parameter a , and upper wall amplitude parameter b .

4.1. Velocity profile

Figs. 2(a)-(d) illustrate a consistent pattern where the maximum velocity is consistently near the center of the channel, and all velocity profiles exhibit a parabolic shape. Figs. 2(a) and 2(b) depict a decrease in velocity profile at the central

part of the channel whereas an increasing effect is noticed toward the boundaries, as well as inflection points appearing via ascending values of Ta and ξ . This outcome arises from the physical phenomenon wherein viscosity decreases as shear rate escalates during rotational motion. As a consequence, its velocity increases. It's worth noting from Fig. 2(c) that as θ enlarges, the fluid velocity reduces. However, an opposite reaction on velocity profile is observed from Fig. 2(d), that means as the phase difference between waves increases (Φ), the axial velocity increases across the entire range of the y -axis.

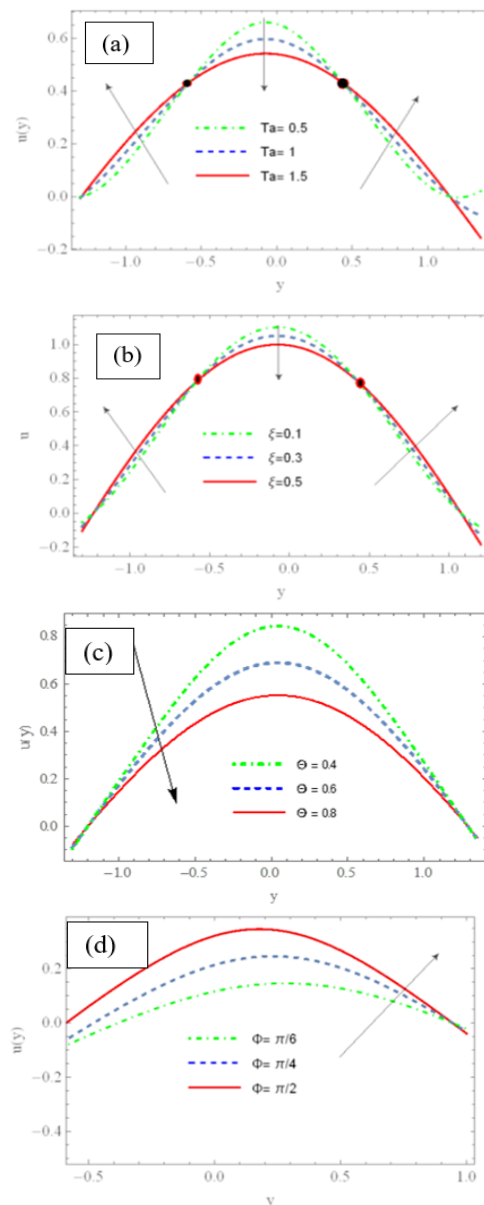


Figure 2. Velocity profile for ascending values of (a) rotation parameter (b) Pseudoplastic parameter (c) non-dimensional mean flows parameter (d) phase difference parameter and fixed $b = 0.3, a = 0.6, x = 0.5, t = 0.2$.

4.2. Gradient of pressure

Figs. 3(a)-(d) record the fluctuations in the axial pressure gradient (dp/dx), exhibiting sinusoidal behavior across the entire x -axis range when it is analyzed under the impact of increasing values of the lower wall wave amplitude a , the rotation parameter Ta , non-dimensional mean flows θ , and the Pseudoplastic fluid parameter ξ . It is noticed from Fig. 3(a) The observed elevation in the magnitude of the pressure gradient towards the central region of the channel compared to its boundaries is attributed to the augmentation of a , leading to an expansion in the dimensions of the channel wall. While from Figs. 3(b) and 3(c), we conclude that the rate of change for (dp/dx) with respect to Ta and θ means the flow can smoothly pass without requiring a significant pressure gradient. Fig. 3(d) illustrated that as ξ increases, a reversal in the situation is depicted, as this parameter inversely correlates with the velocity of the fluid. Consequently, a notable pressure gradient is necessitated to ensure fluid flow remains smooth.

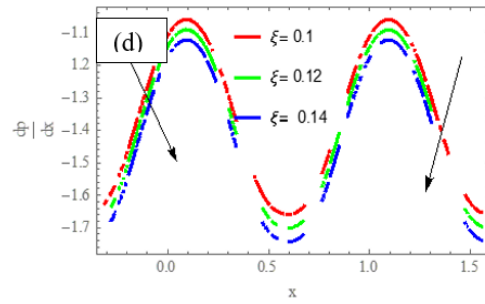
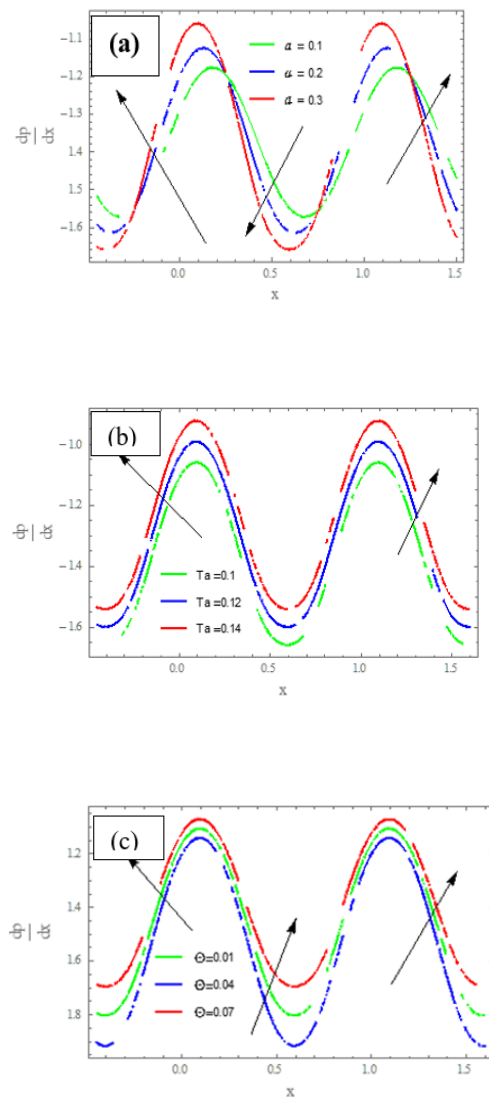
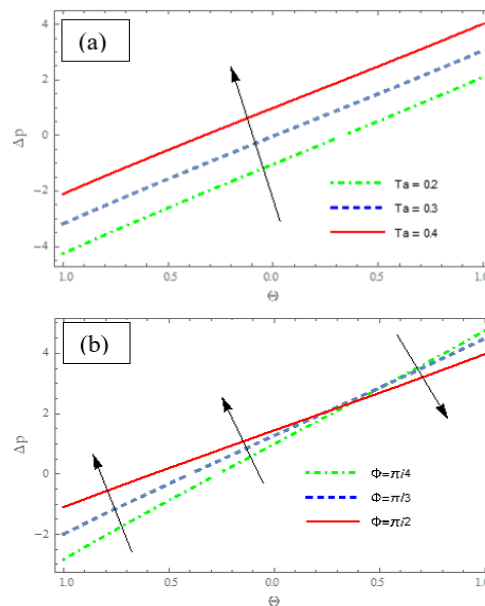


Figure 3. Pressure gradient profile for ascending values of (a) low wall amplitude parameter (b) rotation parameter (c) non-dimensional mean flows parameter (d) Pseudoplastic parameter and fixed $b = 0.3, a = 0.6, x = 0.5, t = 0.2$.

4.3. Pressure rise profile

Figs. 4(a)-(d) elucidate the behavior of nondimensional pressure rise Δp versus the dimensionless mean flow rate θ through plotting Δp profile with various values of the rotation parameter Ta , the phase difference parameter Φ , the lower wall amplitude a , and the upper wall amplitude b . It is clear from Fig. 4(a) that the pumping rate Δp is enlarged in the whole region as the value of Ta is increased. Whereas the impact of enhancing Φ and a on pumping rate anticipated in Figs. 4(b) and 4(c). The plots recorded a decay in peristaltic pumping region with ($\theta > 0, \Delta p > 0$) while an increment impact is noticed in the retrograde pumping area ($\theta < 0, \Delta p > 0$) and no flow area ($\theta < 0, \Delta p < 0$). The opposite scene is depicted with an increasing b , that means the peristaltic pumping region is enhanced while the retrograde pumping and no flow areas are dampened, see Fig. 4(d).



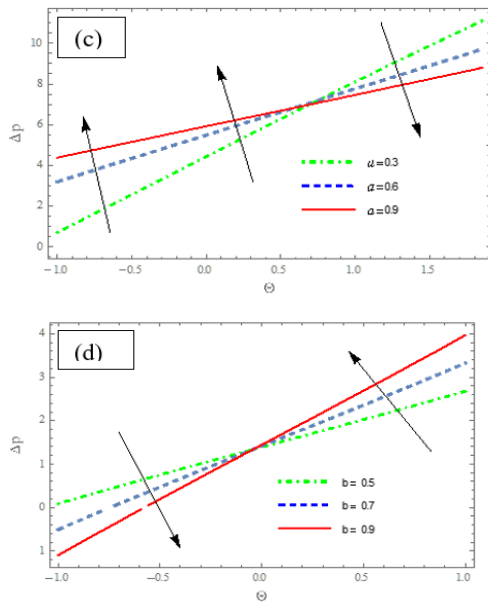


Figure 4. Pressure rise profile for ascending values of (a) rotation parameter (b) phase difference parameter (c) lower wall amplitude parameter (d) upper wall amplitude parameter (d) and fixed $\{\xi = 0.3, \theta = 0.6, x = 0.5, t = 0.2\}$.

4.4. Trapping phenomenon

Streamlines depict the paths followed by fluid particles within a flow. The creation of an enclosed, circulating mass of fluid due to the closed streamlines is referred to as trapping phenomenon. Figs. 5-8 are sketched to elucidate the influence of the rotation parameter Ta , the non-dimensional mean flow parameter θ , the Pseudoplastic fluid parameter ξ , and the phase difference parameter Φ on the absolute value of stream function $|\psi|$. Moreover, we noticed from the graphs that the trapped bolus is composed and focused near the channel's walls. Figs. 5 and 6 illustrate that as the Ta and θ values increase, the trapped bolus size increases. This outcome correlates with the observation that an increase in these parameters leads to a rise in the flow rate, thereby resulting in the generation of more streamlines and boluses. Figs. 7 and 8 reveal a decrease in the size and number of the trapped bolus as the magnitude of ξ and Φ are enlarged. This result aligns well with findings from previous studies conducted by [9] and [19].

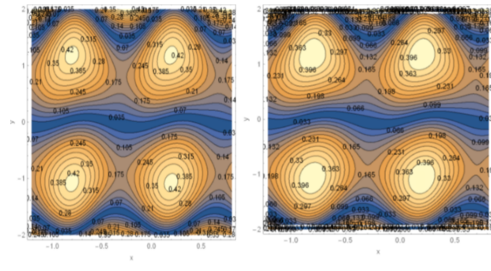


Figure 5. Stream lines for ascending values of rotation parameter $\{Ta = 0.1, Ta = 0.3\}$.

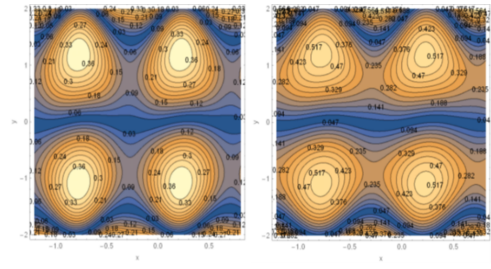


Figure 6. Stream lines for ascending values of rotation parameter $\{\theta = 0.2, \theta = 0.5\}$.

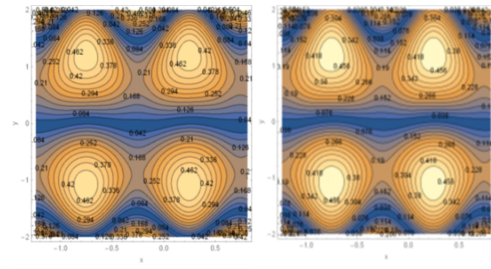


Figure 7. Stream lines for ascending values of pseudoplastic fluid parameter $\{\xi = 0.1, \xi = 0.3\}$.

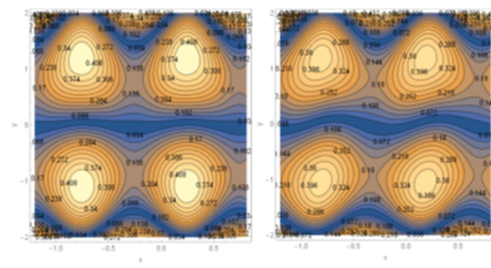


Figure 8. Stream lines for ascending values phase difference parameter $\{\Phi = \pi/6, \Phi = \pi/4\}$.

5. Conclusions

The influence of rotation on peristaltic motion for non-Newtonian pseudoplastic fluid in a wavy channel has yielded significant insights. By modeling and transforming the basic governing equations and employing perturbation method, we

have obtained analytical expressions for key parameters such as stream function, velocity, pressure gradient, and pressure rise. The study has led to several noteworthy findings:

1. The velocity profile exhibits a parabolic shape, with a decrease in velocity profile attributed to an increase in the pseudoplastic fluid parameter ξ . This decrease is due to the shear-thickening effect or reduction in fluid viscosity as the rate of deformation increases, thereby opposing the flow.
2. The velocity profile exhibits a reduction in the central region with increasing rotation parameter Ta and phase difference Φ , while it increases towards the boundaries. This phenomenon arises from the enhancement of kinematic forces induced by rotation, and wave phase difference particularly at the boundaries, thereby accelerating fluid flow.
3. Because of the direct effect of Ta parameter on the fluid velocity, a smooth flow can occur without requiring a significant pressure gradient with increasing Ta and mean flow rate θ , while an opposite trend is observed as ξ increases, necessitating a substantial pressure gradient.
4. The peristaltic pumping region contracts with an increase in the lower wall amplitude a , while it strengthens with an increase in the upper wall amplitude b .
5. The size of the trapped bolus increases with increasing values of Ta and θ , while its volume and number decrease with the magnitude of ξ and Φ .
6. These findings offer valuable insights into the behavior of peristaltic motion in complex fluid systems, with potential applications in various fields such as biomedical engineering, microfluidics, and industrial processes. Understanding these phenomena can aid in the design and optimization of systems involving fluid transport, leading to improved efficiency and performance.

Acknowledgments

The authors would like to thank the editor and anonymous referees for helpful comments and suggestions.


References

- [1] Ali, H. A. (2021). Radiative peristaltic transport of Ree-Eyring fluid through porous medium in asymmetric channel subjected to combined effect of inclined MHD and convective conditions. *In Journal of Physics: Conference Series* (Vol. 1879, No. 2, p. 022101). IOP Publishing. <https://doi.org/10.1088/1742-6596/1879/2/022101>
- [2] Ali, H. A. (2022). Impact of Varying Viscosity with Hall Current on Peristaltic Flow of Viscoelastic Fluid Through Porous Medium in Irregular Microchannel. *Iraqi Journal of Science*, 1265-1276. <https://doi.org/10.24996/ij.s.2022.63.3.31>
- [3] Waseem, F., Sohail, M., Lone, S. A., & Cham-bashi, G. (2023). Numerical simulations of heat generation, thermal radiation and thermal transport in water-based nanoparticles: OHAM study. *Scientific Reports*, 13(1), 15650. <https://doi.org/10.1038/s41598-023-42582-4>
- [4] Li, S., Akbar, S., Sohail, M., Nazir, U., Singh, A., Alanazi, M., & Hassan, A. M. (2023). Influence of buoyancy and viscous dissipation effects on 3D magneto hydrodynamic viscous hybrid nano fluid (MgO-TiO₂) under slip conditions. *Case Studies in Thermal Engineering*, 49, 103281. <https://doi.org/10.1016/j.csite.2023.103281>
- [5] Latham, T. W. (1966). *Fluid motions in a peristaltic pump* (Doctoral dissertation, Massachusetts Institute of Technology).
- [6] Shapiro, A. H., Jaffrin, M. Y., & Weinberg, S. L. (1969). Peristaltic pumping with long wavelengths at low Reynolds number. *Journal of fluid mechanics*, 37(4), 799-825. <https://doi.org/10.1017/S0022112069000899>
- [7] Al-Khafajy, D. G. S., & Noor, A. L. (2022). The peristaltic flow of jeffrey fluid through a flexible channel. *Iraqi Journal of Science*, 5476-5486. <https://doi.org/10.24996/ij.s.2022.63.12.33>
- [8] Salman, M. R., & Ali, H. A. (2020). Approximate treatment for the MHD peristaltic transport of jeffrey fluid in inclined tapered asymmetric channel with effects of heat transfer and porous medium. *Iraqi Journal of Science*, 3342-3354. <https://doi.org/10.24996/ij.s.2020.61.12.22>
- [9] Hayat, T., Iqbal, R., Tanveer, A., & Alsaedi, A. (2018). Variable viscosity effect on MHD peristaltic flow of pseudoplastic fluid in a tapered asymmetric channel. *Journal of Mechanics*, 34(3), 363-374. <https://doi.org/10.1017/jmech.2016.111>
- [10] Nazir, U., Sohail, M., Mukdasai, K., Singh, A., Alahmadi, R. A., Galal, A. M., & Eldin, S. M. (2022). Applications of variable thermal properties in Carreau material with ion slip and Hall forces towards cone using a non-Fourier approach via FE-method and mesh-free study. *Frontiers in Materials*, 9, 1054138. <https://doi.org/10.3389/fmats.2022.1054138>
- [11] Hayat, T., Iqbal, R., Tanveer, A., & Alsaedi, A. (2016). Soret and Dufour effects in MHD peristalsis of pseudoplastic nanofluid with chemical reaction. *Journal of Molecular Liquids*, 220, 693-706.


- <https://doi.org/10.1016/j.molliq.2016.04.123>
- [12] Imran, N., Javed, M., Sohail, M., Qayyum, M., & Mehmood Khan, R. (2023). Multi-objective study using entropy generation for Ellis fluid with slip conditions in a flexible channel. *International Journal of Modern Physics B*, 37(27), 2350316. <https://doi.org/10.1142/S0217979223503162>
- [13] Liu, J., Nazir, U., Sohail, M., Mukdasai, K., Singh, A., Alanazi, M., & Chambashi, G. (2023). Numerical investigation of thermal enhancement using MoS₂-Ag/C₂H₆O₂ in Prandtl fluid with Soret and Dufour effects across a vertical sheet. *AIP Advances*, 13(7). <https://doi.org/10.1063/5.0152262>
- [14] Khan, R. M., Ashraf, W., Sohail, M., Yao, S. W., & Al-Kouz, W. (2020). On behavioral response of microstructural slip on the development of magnetohydrodynamic micropolar boundary layer flow. *Complexity*, 2020, 1-12. <https://doi.org/10.1155/2020/8885749>
- [15] Sohail, M., Alyas, N., & Saqib, M. (2023). Contribution of double diffusion theories and thermal radiation on three dimensional nanofluid flow via optimal homotopy analysis procedure. *Int J Emerg Multidis Math*, 2(1), 2790-3257. <https://doi.org/10.59790/2790-3257.1038>
- [16] Sohail, M., Nazir, U., Naz, S., Singh, A., Mukdasai, K., Ali, M. R., Khan, M. J. & Galal, A. M. (2022). Utilization of Galerkin finite element strategy to investigate comparison performance among two hybrid nanofluid models. *Scientific Reports*, 12(1), 18970. <https://doi.org/10.1038/s41598-022-22571-9>
- [17] Hou, E., Jabbar, N., Nazir, U., Sohail, M., Javed, M. B., Shah, N. A., & Chung, J. D. (2022). Significant mechanism of Lorentz force in energy transfer phenomena involving viscous dissipation via numerical strategy.
- [18] Sohail, M., & Nazir, U. (2023). Numerical computation of thermal and mass transportation in Williamson material utilizing modified fluxes via optimal homotopy analysis procedure. *Waves in Random and Complex Media*, 1-22. <https://doi.org/10.1080/17455030.2023.2226230>
- [19] Tahir, M., & Ahmad, A. (2020). Impact of pseudoplasticity and dilatancy of fluid on peristaltic flow and heat transfer: Reiner-Philippoff fluid model. *Advances in Mechanical Engineering*, 12(12), 1687814020981184. <https://doi.org/10.1177/1687814020981184>
- [20] Hina, S., Hayat, T., Mustafa, M., & Alsaedi, A. (2014). Peristaltic transport of pseudoplastic fluid in a curved channel with wall properties and slip conditions. *International Journal of Biomathematics*, 7(02), 1450015. <https://doi.org/10.142/S1793524514500156>
- [21] Salman, M. R. (2023, February). Effect of convective conditions in a radiative peristaltic flow of pseudoplastic nanofluid through a porous medium in a tapered an inclined asymmetric channel. *In AIP Conference Proceedings* (Vol. 2414, No. 1). AIP Publishing. <https://doi.org/10.1063/5.0117556>
- [22] Alshareef, T. S. (2020). Impress of rotation and an inclined MHD on waveform motion of the non-Newtonian fluid through porous canal. *In Journal of Physics: Conference Series*, 1591(1), 012061. IOP Publishing. <https://doi.org/10.1088/1742-6596/1591/1/012061>
- [23] Abd-Alla, A. M., & Abo-Dahab, S. M. (2016). Rotation effect on peristaltic transport of a Jeffrey fluid in an asymmetric channel with gravity field. *Alexandria Engineering Journal*, 55(2), 1725-1735. <https://doi.org/10.1016/j.aej.2016.03.018>
- [24] Nassief, A. M., & Abdulhadi, A. M. (2023). Rotation and magnetic force effects on peristaltic transport of non-newtonian fluid in a symmetric channel. *Ibn AL-Haitham Journal For Pure and Applied Sciences*, 36(2), 436-453. <https://doi.org/10.30526/36.2.3066>
- [25] Mohaisen, H. N., & Abdalhadi, A. M. (2022). Influence of the induced magnetic and rotation on mixed convection heat transfer for the peristaltic transport of bingham plastic fluid in an asymmetric channel. *Iraqi Journal of Science*, 1770-1785. <https://doi.org/10.24996/ijs.2022.63.4.35>
- [26] Abd-Alla, A. M., & Abdallah, M. (2022). Effect of heat transfer and rotation on the peristaltic flow of a micropolar fluid in a vertical symmetric channel. *Sohag Journal of Sciences*, 7(3), 117-122.
- [27] Salim, S. H., Al-Anbari, R. H., & Haider, A. J. (2021). Polymeric membrane with nanomaterial's for water purification: a review. *In IOP Conference Series: Earth and Environmental Science*, 779(1), 012103. IOP Publishing. <https://doi.org/10.1088/1755-1315/779/1/012103>
- [28] Radhi, A. B., Khashan, K. S., & Sulaiman, G. M. (2023). Antibacterial Activity of Gold Nanoparticles Produced by One-Step Pulsed Laser Ablation in Liquid. *Plasmonics*, 1-13. <https://doi.org/10.1007/s11468-023-02081-8>
- [29] Salman, M. R., & Abdulhadi, A. M. (2018, May). Influence of heat and mass transfer on inclined (MHD) peristaltic of pseudoplastic nanofluid through the porous medium with couple stress in an inclined asymmetric channel. *In Journal of Physics: Conference Series* (Vol. 1032, No. 1, p. 012043). IOP Publishing. <https://doi.org/10.1088/1742-6596/1032/1/012043>
- [30] Khan, R. M., Imran, N., Mehmood, Z., & Sohail, M. (2022). A Petrov-Galerkin finite element approach for the unsteady boundary layer upper-convected rotating Maxwell fluid flow and heat transfer analysis. *Waves in Random and Complex Media*, 1-18. <https://doi.org/10.1080/17455030.2022.2055201>
- [31] Ali, U., Alqahtani, A. S., Rehman, K. U., & Malik, M. Y. (2019). On Cattaneo-Christov heat flux

- analysis with magneto-hydrodynamic and heat generation effects in a Carreau nano-fluid over a stretching sheet. *Revista mexicana de física*, 65(5), 479-488. <https://doi.org/10.31349/RevMexFis.65.479>
- [32] Bibi, M., Zeeshan, A., Malik, M. Y., & Rehman, K. U. (2019). Numerical investigation of the unsteady solid-particle flow of a tangent hyperbolic fluid with variable thermal conductivity and convective boundary. *The European Physical Journal Plus*, 134, 1-10. <https://doi.org/10.1140/epjp/i2019-12651-9>
- [33] Rehman, K. U., Malik, M. Y., Makinde, O. D., & Malik, A. A. (2017). A comparative study of nanofluids flow yields by an inclined cylindrical surface in a double stratified medium. *The European Physical Journal Plus*, 132(10), 427. <https://doi.org/10.1140/epjp/i2017-11679-1>
- [34] Rehman, K. U., Al-Mdallal, Q. M., Tlili, I., & Malik, M. Y. (2020). Impact of heated triangular ribs on hydrodynamic forces in a rectangular domain with heated elliptic cylinder: finite element analysis. *International Communications in Heat and Mass Transfer*, 112, 104501. <https://doi.org/10.1016/j.icheatmasstransfer.2020.104501>
- [35] Rehman, K. U., Shatanawi, W., & Al-Mdallal, Q. M. (2022). A comparative remark on heat transfer in thermally stratified MHD Jeffrey fluid flow with thermal radiations subject to cylindrical/plane surfaces. *Case Studies in Thermal Engineering*, 32, 101913. <https://doi.org/10.1016/j.csite.2022.101913>
- [36] Abass, G., & Shihab, S. (2023). Operational Matrix of New Shifted Wavelet Functions for Solving Optimal Control Problem. *Mathematics*, 11(14), 3040. <https://doi.org/10.3390/math11143040>
- [37] Aydin, C., & Tezer-Sezgin, M. (2019). The DRBEM solution of Cauchy MHD duct flow with a slipping and variably conducting wall using the well-posed iterations. *An International Journal of Optimization and Control: Theories & Applications (IJOCTA)*, 9(3), 76-85. <https://doi.org/10.11121/ijocta.01.2019.00677>

Hayat Adel Ali is full professor in applied mathematics at the Department of Mathematics and Computer Application, University of Technology-Iraq. My research interests include numerical analysis and fluid mechanic.

 <https://orcid.org/0000-0002-0368-0764>

Mohammed R. Salman is an assistance professor in fluid mechanics at the Department of Mathematics, College of Education for Pure Sciences, University of Karbala, Iraq. His research interest includes fluid mechanics.

 <https://orcid.org/0000-0001-9611-4544>

An International Journal of Optimization and Control: Theories & Applications (<http://www.ijocta.org>)



This work is licensed under a Creative Commons Attribution 4.0 International License. The authors retain ownership of the copyright for their article, but they allow anyone to download, reuse, reprint, modify, distribute, and/or copy articles in IJOCTA, so long as the original authors and source are credited. To see the complete license contents, please visit <http://creativecommons.org/licenses/by/4.0/>.